A Pilot Imaging Line Survey of RW LMi and IK Tau Using the Expanded Very Large Array

M. J Claussen, L. O. Sjouwerman, M. P. Rupen

National Radio Astronomy Observatory, Socorro, New Mexico 87801

H. Olofsson, F. L. Schöier[1], P. Bergman

Onsala Space Observatory, Dept. of Radio and Space Science, Chalmers University of Technology, 43992 Onsala, Sweden

G. R. Knapp[2]

Department of Astrophysical Sciences, Princeton University, Princeton, NJ 08544

ABSTRACT

We report on a pilot imaging line survey (36.0 - 37.0 GHz, with $\sim$1 km s^{-1} spectral channels) with the Expanded Very Large Array for two asymptotic giant branch stars, RW LMi (= CIT6, which has a carbon-rich circumstellar envelope) and IK Tau (= NML Tau, with an oxygen-rich circumstellar envelope). Radio continuum emission consistent with photospheric emission was detected from both stars. From RW LMi we imaged the HC_3N (J = 4$\rightarrow$3) emission. The images show several partial rings of emission; these multiple shells trace the evolution of the CSE from 400 to 1200 years. SiS (J = 2$\rightarrow$1) emission was detected from both RW LMi and IK Tau. For both stars the SiS emission is centrally condensed with the peak line emission coincident with the stellar radio continuum emission. In addition, we have detected weak HC_7N (J = 32$\rightarrow$31) emission from RW LMi.

Subject headings: Stars: AGB and post-AGB — Stars: individual (RW LMi, IK Tau) — Radio continuum: stars — Radio lines: stars

[1]deceased

[2]Visiting Astronomer, NRAO

1. Introduction

The extensive mass loss which occurs from stars on the asymptotic giant branch (AGB) leads to the formation of dusty, extended, circumstellar envelopes (CSE) and the production of many gas-phase molecular species in the atmospheres and CSE (e.g. Olofsson 2008). The CSEs of AGB stars eventually contribute their heavy elements and dust grains back to the interstellar medium (ISM). Molecules from the CSE may be returned directly to the ISM or by incorporation into or onto the dust grains.

Mass loss from AGB stars can be as high as 10^{-4} $M_{\odot}$ yr^{-1} or even higher (Habing 1996) and is the dominant process at this stage of evolution. It determines the stellar lifetime on the AGB, the maximum luminosity reached, the post-AGB evolution of the star, the gas and dust return to the ISM, and the chemical composition of the returned gas (Bloecker 1995). Although the mass loss mechanism is complex and dependent on many different physical and chemical processes, the reasonably simple geometry and kinematics of the resulting CSEs make them excellent astrophysical and astrochemical laboratories.

Interferometric imaging of thermal molecular emission in CSEs have been mostly confined to the nearby carbon-rich object IRC+10°216, which has a very high mass-loss rate, although there have been targeted imaging projects of other sources. If we are interested in a much better understanding of circumstellar chemistry, we must observe more typical sources, compare oxygen- and carbon-rich CSEs, use high-sensitivity interferometry to provide detailed images of the molecular line distribution, and cover a large number of molecular species transitions. To do all these successfully one line at a time (or even a few) would be prohibitive in terms of telescope time. Thus an interferometric imaging line survey, as being carried out by the Submillimeter Array (Patel et al. 2011) is required.

In this short *Letter* we report on a project that is a pilot for observations of such an imaging line survey using the Expanded Very Large Array (EVLA; Perley et al. 2011). We proposed to observe one each of a carbon-rich CSE (RW LMi = CIT6), an oxygen-rich CSE (IK Tau = NML Tau), and an S-type AGB star (χ Cyg). At the time of observations, the WIDAR correlator could process a maximum of 1 GHz bandwidth per polarization with spectral channels of $\sim$1 km s^{-1} at the Ka receiver band (26.5 — 40 GHz). We were unable to observe χ Cyg because necessary Local Sidereal Time (LST) coverage was unavailable.

2. Observations and Data Reduction

IK Tau and RW LMi were observed with the EVLA in the **C** configuration during 2010 December and 2011 January. Each target was observed using four dynamic scheduling blocks

(observing runs) of 3.5 hours, yielding a total of about 7 hours on source integration time each with a fixed frequency setting simultaneously covering 36.000 to 36.512 and 36.744 to 37.000 GHz. For each subband of 128 MHz bandwidth, 1024 channels with a channel separation of 125 kHz ($\sim$ 1 km s^{-1}) were produced. Due to limitations during the early commissioning phase, the full one-GHz range was not available at this resolution, and a relatively large amount of time was spent on additional calibration. For IK Tau, 3C 48 was used for absolute flux calibration, 3C 84 for bandpass and delay calibration, and J0409+1217 for gain (amplitude and phase) calibration. For RW LMi, 3C 286 was used for absolute flux calibration, 3C 273 for bandpass and delay calibration, and J0958+3224 for gain calibration.

Standard data editing, flux, bandpass and phase calibration were performed using AIPS and a modified version of the VLA pipeline. The four data chunks per source were combined using the strongest line by correcting for the approximate Doppler shift for the day of observation, although the diurnal variation was ignored for these short observations. The maximum shifts applied were 5 and 8 channels for IK Tau and RW LMi, respectively. Before imaging all individual channels using natural weighting and 0.165″ pixel size without cleaning, the data were averaged to 20 second visibilities and separated by subband, which speeds up the process considerably. The continuum emission and spectral channels containing interesting spectral line features were selected and re-imaged with cleaning.

The synthesized beams from the imaging were $\sim$0.7 x 0.6 arcseconds, depending slightly upon the frequency and the source. The typical rms noise in a single 125 kHz spectral channel is $\sim$500 μJy beam^{-1}, and $\sim$10 μJy beam^{-1} in the continuum.

3. Results

Radio continuum emission at $\sim$36.5 GHz was detected from both IK Tau (970$\pm$10 μJy beam^{-1}) and RW LMi (890$\pm$10 μJy beam^{-1}).

Line emission was detected from the HC_3N (J = 4$\rightarrow$3; rest frequency 36392.332 MHz), the SiS (J = 2$\rightarrow$1; 36309.627 MHz), and the HC_7N (J = 32$\rightarrow$31; 36095.546 MHz) transitions in the carbon-rich CSE in RW LMi. The only spectral line clearly detected in IK Tau was the SiS (J = 2$\rightarrow$1 transition, although the total frequency coverage included the SO (J, N = (2,3)$\rightarrow$(2,2); 36202.041 MHz) transition, and the OCS (J = 3$\rightarrow$2; 36488.813 MHz) transition.

Figure 1 shows the emission in nine of the 34 velocity images of the HC_3N line from RW LMi. These images show striking concentric rings in the HC_3N emission; very clear evidence of multiple spherical shells of emission. In the large-scale structure of the ring

emission, there are also noticeable asymmetries — in the west and northwest near the central velocities, and to the east in more blue-shifted velocities. The EVLA data is more sensitive at higher angular and spectral resolution than the spectrally averaged HC_3N ($J = 5 \rightarrow 4$) data from the VLA at 45.5 GHz presented by Dinh-V-Trung & Lim (2009). The similarities of the two data sets are striking in terms of asymmetries; however the higher sensitivity EVLA images show a wealth of detail (e.g. the several emission shells) not found in the VLA data.

Figure 2 shows images of the continuum-subtracted, averaged (in velocity) emission of the SiS line from both RW LMi and IK Tau (all channel images showing emission were averaged together after subtracting the continuum in the u-v data). As compared with the HC_3N emission, the SiS emission from RW LMi is more compact, centrally condensed, but slightly elongated in the N-S direction. For IK Tau the SiS emission is also centrally concentrated toward the star, and is also elongated rather than circular.

Although we detected the HC_7N line in RW LMi, the emission is quite weak, and further analysis of this transition will be deferred to another publication.

Figure 3 shows the global emission of the HC_3N and SiS lines from RW LMi. These spectra were made by summing the emission in the same rectangular region of each spectral channel image. The channel with the largest emission extent was used to set the rectangular region for each line. The spectra for both the SiS and HC_3N lines are clearly asymmetric with the red-shifted side being the brightest.

4. Discussion

4.1. Radio Continuum Emission

At submillimeter and infrared wavelengths the continuum emission from AGB stars is dominated by warm circumstellar dust which has a very steep spectral index (Draine 2006 and references therein). We compared the detections of the radio continuum emission at 36.5 GHz with measurements of other authors at different frequencies. Marshall et al. (1992) observed both RW LMi and IK Tau at frequencies of 264, 394, and 685 GHz. They find the derived spectral index from 100 μm (using *IRAS* data) through 1.1 mm to be $\alpha = -3.9$ (IK Tau) and -3.5 (RW LMi). At centimeter wavelengths emission from dust is small compared to that from the radio "photosphere" (Reid & Menten 1997) i.e. blackbody emission from or just outside the stellar photosphere with a temperature approximately 2000 K, and with a spectral index near -2.0.

Radio continuum measurements of RW LMi at $\sim$3 mm or longer include 13.3 mJy

beam^{-1} at 112 GHz (Neri et al. 1998), 8 mJy at 90.7 GHz (Lindqvist et al. 2000), and 2.4 mJy beam^{-1} at 43.3 GHz (Dinh-V-Trung & Lim 2009). A two-point spectral index derived from 36.5 GHz to 90.7 GHz and from 36.5 GHz to 112 GHz is consistent and equal to $\alpha = -2.3$. The spectral index of 2.3 is reasonably close to that of thermal blackbody radiation. Spectral indices calculated using the flux measured at 43.3 GHz to both higher and lower frequencies are inconsistent and do not fit either photospheric emission or dust emission. All other existing continuum data agree with either photospheric or dust emission, and in particular the present EVLA measurements are likely detecting the photosphere of RW LMi.

A radio continuum measurement of IK Tau at 96.7 GHz of 6.1 mJy beam^{-1} was reported by Marvel (2005). The measurement presented here, combined with Marvel's, produce a two-point spectral index of -2.0. This is just what is expected from a radio photosphere emitting as a blackbody.

4.2. Line Emission

4.2.1. HC_3N Emission in RW LMi

We used the AIPS task IRING to azimuthally sum the HC_3N emission in RW LMi in continuous rings of a fixed width centered on the continuum, for each velocity channel. Using this method we then measured the angular radii of the flux density peaks (rings in Figure 1) in each channel. Assuming that we then can follow the radius of each ring in different channels we can plot, for each detected ring, the radius versus the (LSR) velocity for each ring. Based on this preliminary analysis, we distinguished four such rings of emission; a more careful examination of the channel images in conjunction with the ring analysis is certainly required. The plot of radius versus velocity is shown in Figure 4. The radius in arcseconds is transformed to the radius in AU using a distance of 440 pc (Schöier et al. 2002).

If the rings of emission actually correspond to spherical shells of molecular emission around the star, the radius of the shell as a function of radial velocity is given by

$$r\left(v - v_*\right) = r_0\sqrt{1 - \left(\left(v - v_*\right)/v_{exp}\right)^2}$$

where v_* is the stellar radial velocity, r_0 is the shell radius, and v_{exp} is the constant expansion velocity for a given shell (e.g. Bowers et al. 1983). We fit this equation to the data obtained for the four HC_3N shells as shown in Figure 4, using a simple least-squares method, and using v_*, r_0, and v_{exp} as (bounded) free parameters in the fit. The parameters for each of the shells are listed in Table 1. For comparison, the expansion velocity and stellar radial velocity

are determined to be 17 km s^{-1} and −1.0 km s^{-1} (with respect to the LSR), respectively, based on ^{13}CO observations (Schöier & Olofsson 2000), and the expansion velocity estimated from the spectra in Figure 3 is also 17 — 18 km s^{-1}.

Given the expansion velocity and the radius, a time can be derived which is the approximate age of the shell. This age is also listed in Table 1. The age of shell 3 (from Table 1; blue symbols in Figure 4) is essentially the same as the age of shell 2 (red symbols in Figure 4) — this is clearly because the fit from the data for shell 3 gives a much larger expansion velocity than that from shell 2. We speculate that since these two shells have the same age, they may have a common origin. If so, this would suggest a rather complex behavior in the mass-loss history for RW LMi.

These fitted parameters are only approximate, since it is not always clear how to associate the data into rings. (The red symbols in Figure 4 are an example of this.) Also, the equation above (essentially an ellipse) does not fit the blue-shifted side of the data very well: note that the data on the blue-shifted side of Figure 4 are quite linear as compared to the data on the red-shifted side (which are fit by the velocity equation much better). Perhaps a better way of saying this is that, except for shell 1 (which does not have much emission on the red-shifted side) the data, if extended to the shell center, would intersect 0 AU at approximately the same LSR velocity (∼+13 km s^{-1}). The extensions of the data for the different shells on the blue-shifted side would not intersect 0 AU close to the same velocity at all. We note that the velocity of +13 km s^{-1} corresponds to the velocity in both the spectra in Figure 3 where the steepest part of the spectrum begins. We also point out that full width at zero power (FWZP) of both the SiS and HC_3N lines are essentially the same, despite the fact that the spatial distribution and extent is much different. This suggests that the gas is accelerated quickly in the inner region of the CSE to the expansion velocity. The strong asymmetric character (with the red-shifted side stronger) of both these transitions as well as others (e.g. the SiS, J = 5→4 transition; Lindqvist et al. 2000) must provide clues to detailed kinematics of the gas.

While in general it is clear from Figure 1 that the HC_3N emission from RW LMi consists mostly of broken rings (or shells) of emission, there are some velocity channels which, if the emission is traced carefully, might be considered as a spiral shape (c.f. the velocity channel at −7.5 km s^{-1} in Figure 1). Dinh-V-Trung & Lim suggested such a spiral for the 45.5 GHz transition and there is at least one beautiful example of spiral **dust** emission in a CSE (AFGL 3068; Mauron & Huggins 2006), but if there is such a spiral in our images it has the opposite handedness than that shown in the discussion of Dinh-V-Trung & Lim. Thus we think that the possibility of molecular spiral emission in RW LMi is unlikely, though we do not completely rule it out.

Dinh-V-Trung & Lim (2008) have used high angular resolution observations using the VLA to trace several incomplete arcs (or shells) of HC_3N emission (at the 45.5 GHz transition) and HC_5N emission (transitions at 42.6 and 24.0 GHz) in the prototypical AGB carbon star IRC+10°216, similar to what we have observed in RW LMi. Dinh-V-Trung & Lim (2008) estimate the kinematic timescale between the shells is in the range of ∼120 to ∼360 yr. This is also similar to the timescales shown in Table 1, based on our data for RW LMi. The molecular arcs in IRC+10°216 appear to coincide closely with the dust arcs shown by Mauron & Huggins (2000). For RW LMi, Schmidt et al. (2002) have discovered several faint diffuse arcs of reflected light using deep HST NICMOS imaging. These arcs appear at radial distances of 1.0, 1.3, 3.8, and 4.5 arcseconds from the star, and are most prominent to the south-southwest of the star. Only one of these reflected light arcs may be coincident with the HC_3N shell (at 4.5 arcseconds radius) based on angular radius alone. In addition, as can be seen in Figure 1, the most prominent parts of the rings seen in HC_3N are typically not in the south-southwest part of the images.

4.2.2. SiS Emission in RW LMi and IK Tau

Figure 2 shows the SiS emission from both AGB stars averaged over the line. We note that there is a large difference in angular size of the SiS emission between the two stars. This may be only a result of the generally weaker emission in IK Tau, but the angular size difference is striking, and, assuming a distance to IK Tau of 250 pc (Olofsson et al. 1998), the total physical extent of the SiS emission is different by a factor 4 (the emission in RW LMi — ∼2000 AU is 4 times larger than in IK Tau — ∼500 AU). The peak of the SiS emission is coincident with that of the radio continuum emission which defines the stellar position.

The size estimate for RW LMi is consistent with the modelling of the SiS molecular abundance by Schöier et al. (2007). The total SiS envelope size based on their Table 3 is ∼1700 AU. The modelling is based on single-dish spectra; however, for RW LMi the model appears to fit the interferometric data from the SiS, J = 5→4 transition at ∼90.7 GHz (Lindqvist et al. 2000) rather well. For IK Tau, the model gives a total SiS envelope size of 2200 AU (a factor 4 larger than our measurement). Schöier et al. point out that their single-Gaussian abundance distribution gives a poor fit to the mm and submm-wave spectra of SiS for IK Tau. The addition of a compact, high abundance component to the model improves the fit, especially for higher J transitions. We speculate that the oxygen-rich chemistry of IK Tau may have some bearing on the detailed radial abundance of SiS in oxygen-rich CSE. It is clear that a larger sample of stars (both oxygen-rich and carbon-rich CSEs) observed with interferometric imaging at high angular resolution are needed to provide the best constraints

on such models.

5. Summary

We have used the ever-growing capabilities of the Expanded Very Large Array to perform a ∼1 GHz, targeted line survey of two AGB stars with ∼1 km s^{-1} spectral resolution (125 kHz at 18 - 50 GHz) and sub-arcsecond angular resolution. The stars are: RW LMi (with a carbon-rich CSE), and IK Tau (with an oxygen-rich CSE). We find the following results in a preliminary analysis of the data:

• Continuum emission from both stars detected at 36.5 GHz is consistent with photospheric emission from thermal gas.

• The HC_3N (J = 4→3) emission from RW LMi is bright enough to be imaged in detail and shows strong asymmetries in the global line profile and partial rings (shells) of emission. We have provided a preliminary analysis of the shell emission and find that the multiple shells can be traced from about 400 years to 1200 years. In addition, we have detected weak HC_7N (J = 32→31) emission from RW LMi.

• The SiS (J = 2→1) emission from both stars is compact, compared with the HC_3N emission from RW LMi. The emission seems elongated for both stars rather than ring-like. The extent of the detected SiS emission in IK Tau is only one-quarter (∼500 AU) that of RW LMi (∼2000 AU) The SiS global line profile from RW LMi is also strongly asymmetric and in the same sense (red-shifted side stronger than blue-shifted side) as the HC_3N line.

By the end of the EVLA construction period (in early 2013) spectral imaging surveys should be able to use 8 GHz per polarization with 125 kHz resolution (or better) in the WIDAR correlator simultaneously. Thus the 3 receiver bands which span the 18 - 50 GHz range could be covered with 5 frequency settings. This will lead to a revolution in spectral imaging surveys of cm molecular transitions in AGB stars and related objects.

It is with sadness that we note the passing earlier this year of our colleague Fredrik Schöier, and we dedicate this short communication in his honor.

The National Radio Astronomy Observatory is a facility of the National Science Foundation operated under cooperative agreement by Associated Universities, Inc.

Facilities: EVLA.

REFERENCES

Bloecker, T. 1995, A&A, 297, 727

Bowers, P. F., Johnston, K. J., & Spencer, J. H. 1983, ApJ, 274, 733

Habing, H. 1996, ARA&A, 7, 978

Dinh-V-Trung & Lim, J. 2008, ApJ, 558, 204

Dinh-V-Trung & Lim, J. 2009, ApJ, 701, 292

Draine, B. T. 2006, ApJ, 636, 1114

Marshall, C. R., Leahy, D. A., & Kwok, S. 1992, PASP, 104, 397

Marvel, K. B. 2005, AJ, 130, 261

Lindqvist, M., Schöier, F. L., Lucas, R., &Olofsson, H. 2000, A&A, 361, 1036

Mauron, N. & Huggins, P. J. 2000, A&A, 359, 707

Mauron, N. & Huggins, P. J. 2006, A&A, 452, 257

Neri, R., Kahane, C., Luca, R., Bjuarrabal, V., Loup, C. 1998, A&AS, 130, 1

Olofsson, H., Lindqvist, M. Nyman, L-Å., Winnberg, A. 1998, A&A, 329, 1059

Olofsson, H. 2008, Ap&SS, 313, 201

Patel, N. A. et al. 2011, ApJS, 193, 17

Perley, R. A., Chandler, C. J., Butler, B. J., & Wrobel, J. M. 2011, ApJ, this issue.

Reid, M. J. & Menten, K. M. 1997, ApJ, 476, 727

Schmidt, G. D., Hines, D. C., & Swift, S. 2002, ApJ, 576, 429

Schöier, F. L. & Olofsson, H. 2000, A&A, 359, 586

Schöier, F. L., Ryde, N., & Olofsson, H. 2002, A&A, 391, 577

Schöier, F. L., Bast, J., Olofsson, H., & Lindqvist, M. 2007, A&A, 473, 871

Table 1: Fitted and Derived Parameters of Possible HC_3N Shells in RW LMi

Shell	v_* (km s^{-1})	r_0 (AU)	v_{exp} (km s^{-1})	Age (yr)
1	-2.6	880	11.3	370
2	-3.1	2000	12.0	800
3	-2.0	2500	15.2	780
4	-1.2	3650	14.8	1200

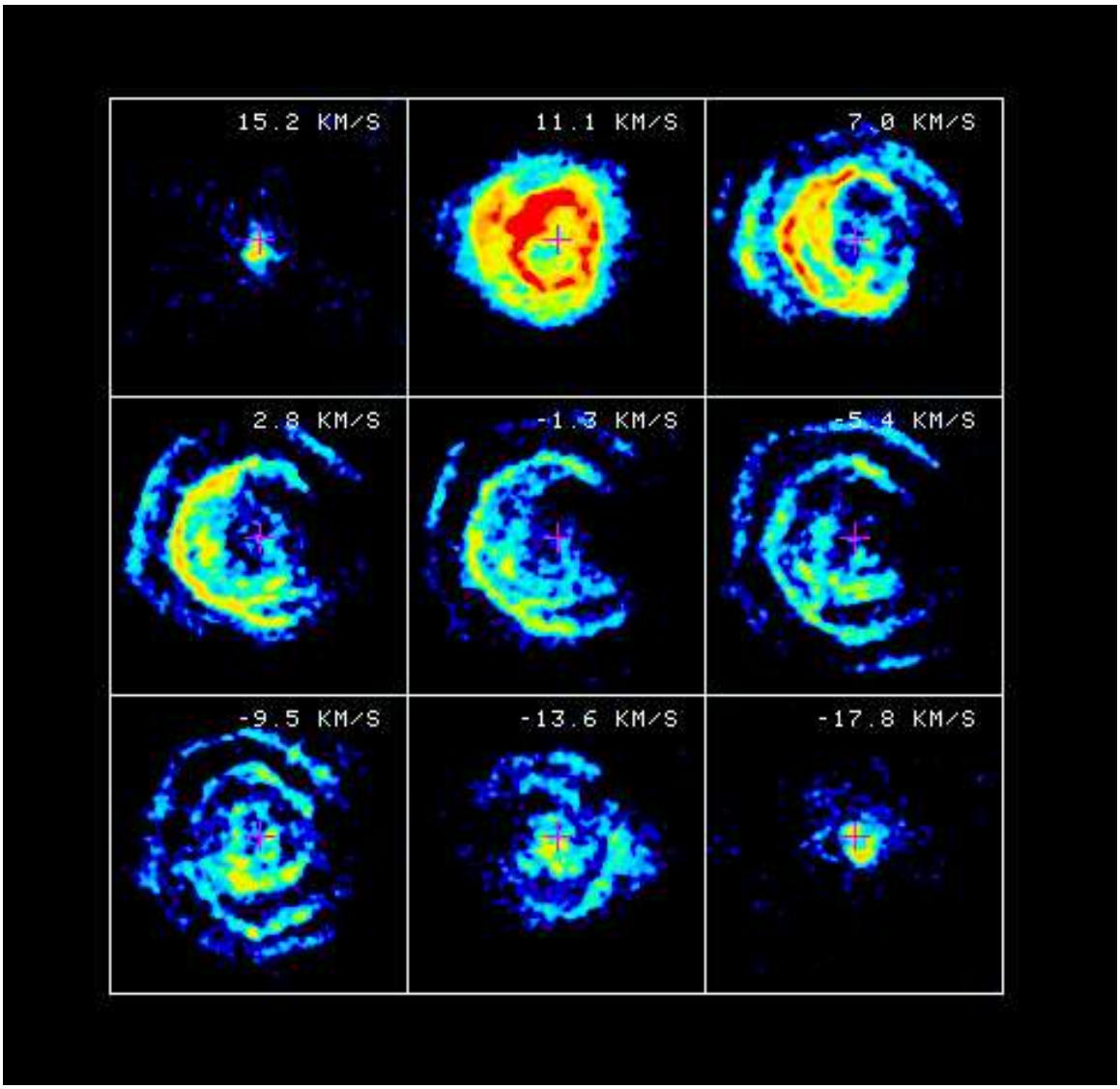

Fig. 1.— Selected channel images of the HC_3N (J = 4→3, rest frequency 36392.332 MHz) emission from RW LMi. This selection spans the range of emission for the HC_3N transition, and each panel is every fourth channel. Each image is ∼21 arcseconds on a side and is labeled with the velocity with respect to the LSR. The cross marks the position of the continuum source; the size of the cross is about ten times the position error of the continuum measurement. North is up and east is to the left.

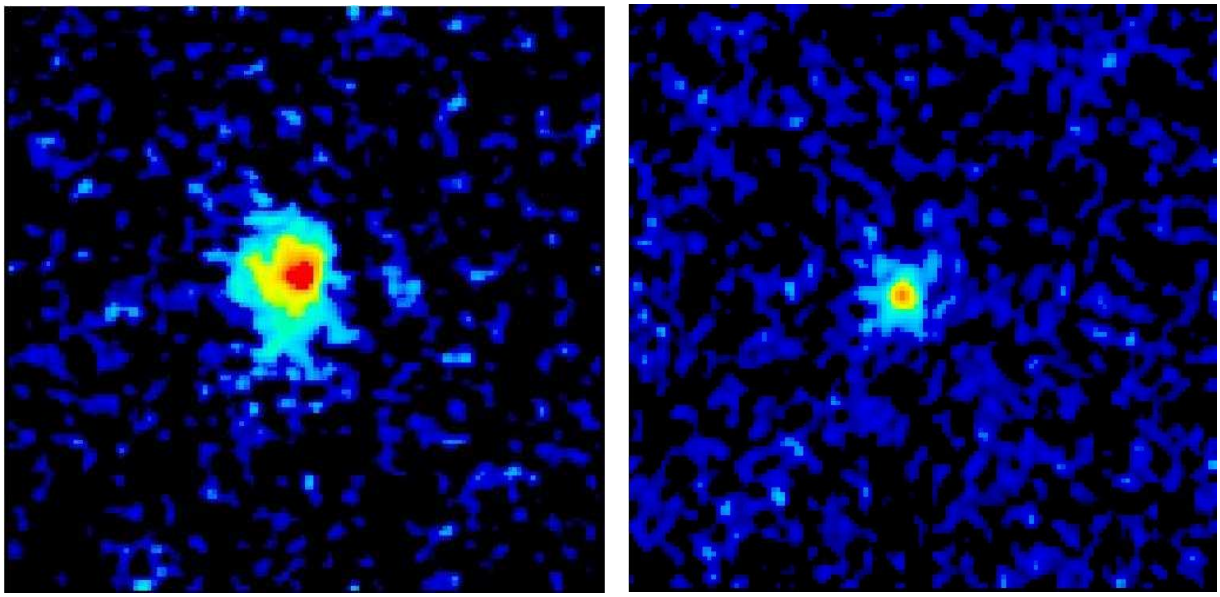

Fig. 2.— The SiS (J=2→1) emission for both sources, averaged over the emission line, and after subtracting the continuum emission. Each panel is ∼21 arcseconds on a side; north is up and east is to the left. Left: the emission from RW LMi. Right: the emission from IK Tau.

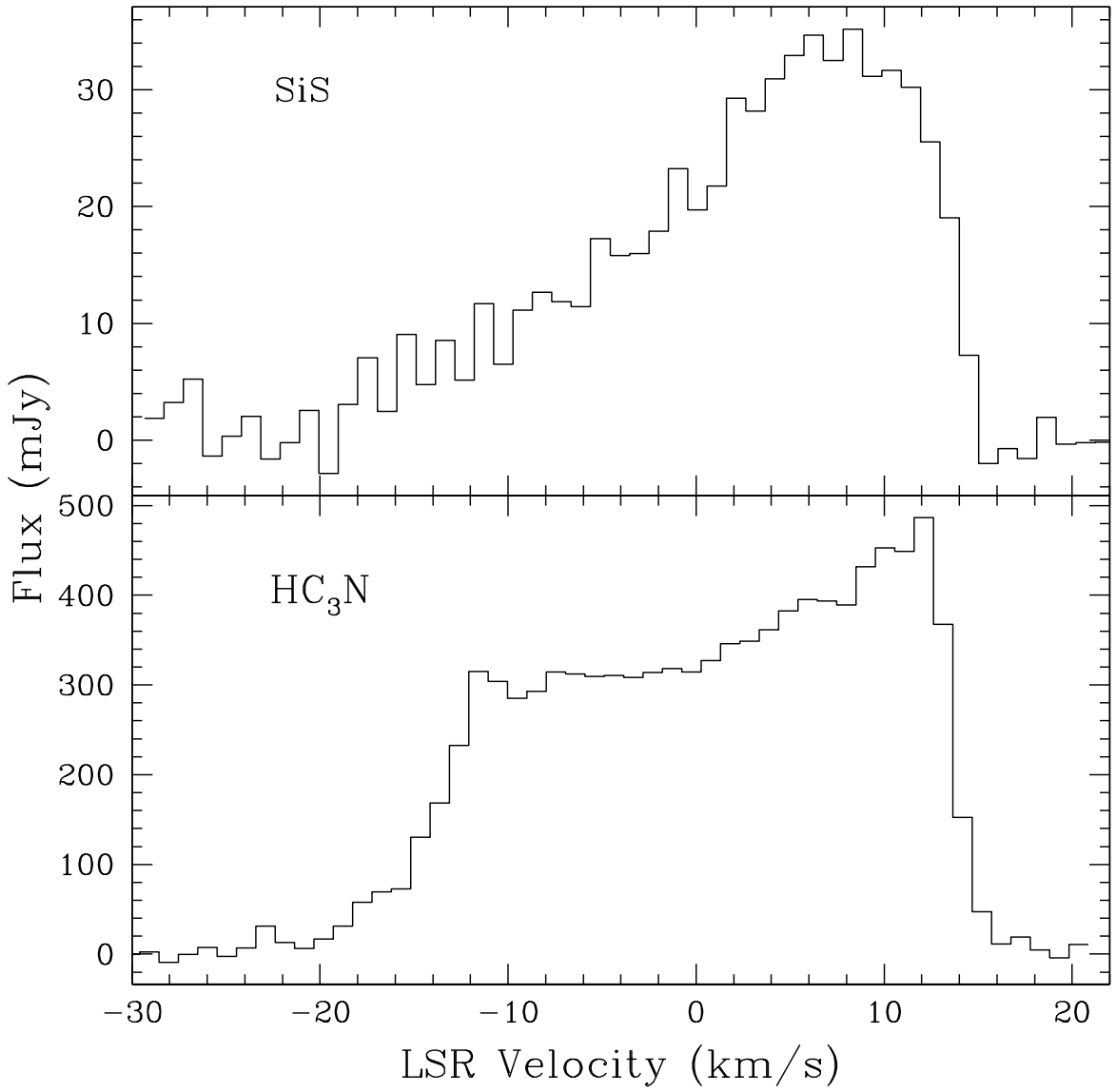

Fig. 3.— Spectra of the HC_3N (J = 4→3) line (bottom) and the SiS (J = 2→1) line (top) from RW LMi. The spectra were produced by summing the emission in a give rectangular region for each spectral channel (the summed region is much smaller for the SiS line as compared with the HC_3N line).

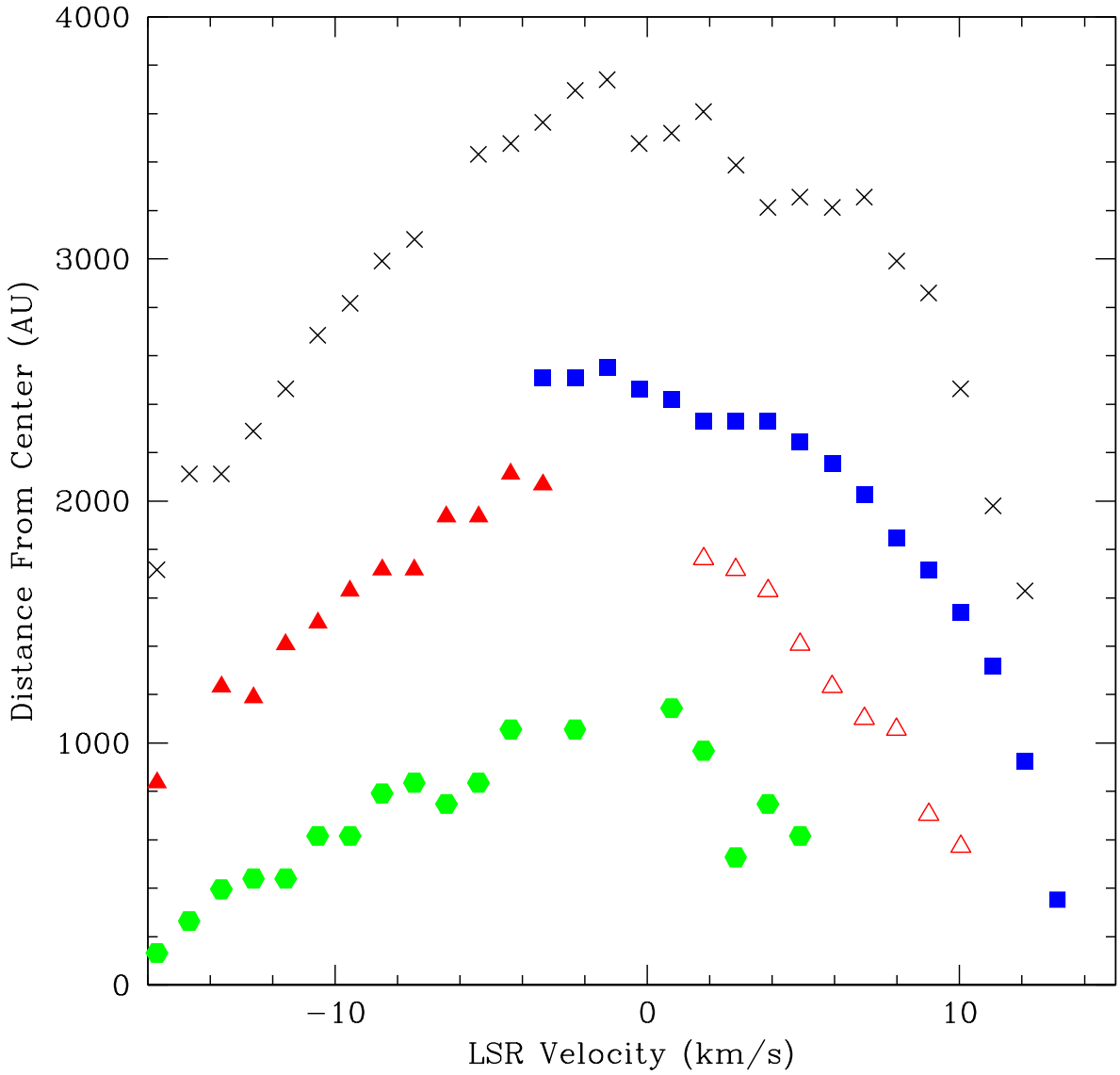

Fig. 4.— Plots of the radius vs. LSR velocity for the shells of the HC_3N emission in RW LMi, as determined using the IRING task of AIPS (which integrates the emission in azimuthal rings for each channel). The errors in the distance of these rings are approximately the size of the symbols. The different sections of the red triangles (one section is solid; one is open) may or may not be the same ring, since it is difficult to determine, given the general asymmetric nature of the emission (see Figure 1 and the text).